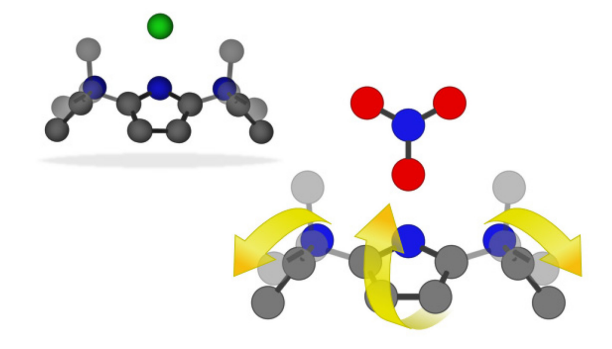
Effects of Anion Size, Shape, and Solvation in Binding of Nitrate to Octamethyl Calix[4]Pyrrole

Lane M. Terry, Madison M. Foreman, and J. Mathias Weber^{a,*}

^a JILA and Department of Chemistry, University of Colorado, 440 UCB, Boulder, CO 80309-0440, USA.

ABSTRACT. We present cryogenic ion vibrational spectroscopy of complexes of the anion receptor octamethyl calix[4]pyrrole (omC4P) with nitrate in vacuo. We compare the resulting vibrational spectrum with that in deuterated acetonitrile solution, and we interpret the results using density functional theory. Nitrate binds to omC4P through H-bonds between the four NH groups of the receptor and a single NO group of the nitrate ion. The shape of the ion breaks the C_{4v} symmetry of the receptor, and this symmetry lowering is encoded in the pattern of the NH stretching modes of omC4P. We compare the spectrum of nitrate-omC4P with that of chloride-omC4P to discuss effects of ion size, shape, and solvent interaction on the ion binding behavior.

TOC Graphic



Anion receptors have multiple applications in chemistry,¹⁻⁵ e.g., in the regulation of anion concentrations in living systems⁶⁻⁹ and in sensing of anionic pollutants from agricultural, industrial, or military sites.¹⁰⁻¹³ Anion binding to such receptors relies on non-covalent interactions between the ions and the receptor binding site, which are in competition with solvation effects. This competition makes a quantitative, predictive characterization of anion binding rather difficult, and the detailed understanding of the competing effects remains a frontier in the supramolecular chemistry of anionic guests binding to molecular hosts, with the ultimate aim of designing efficient and selective anion receptors for a given anion.^{3, 14, 15} The binding site is often formed by a cavity whose size and shape determines the binding geometry for the ion in question, as well as the exposure of the ion to solvent molecules. These factors are crucial for the binding efficiency and selectivity of an ion receptor.

Out of the many classes of natural and artificial anion receptors, calix[4]pyrroles have received particular attention over the past two decades.^{3, 9, 16-25} First synthesized by Baeyer in 1886²⁶ and rediscovered as anion receptors by Sessler around 2000, ^{16, 20, 21, 27} octamethyl calix[4]pyrrole (omC4P) represents the simplest version of these synthetic anion receptors, consisting of four pyrrole rings that are connected by substituted sp³ *meso*-carbon bridges and arranged in a macrocycle (see Figure 1). In the presence of anions, the NH groups of the pyrrole rings form a pyramidal structure, generating a binding site that can capture anions through four hydrogen bonds (H-bonds). At the same time, the pyrrole rings form a concave binding site for cations, facilitating ion pair binding, particularly in less polar solvents.²³

The interaction of the anion guest with the omC4P host is dominated by the H-bonds between the NH groups and the ion. The NH stretching modes are very sensitive to this interaction, and they represent excellent probes for the binding of a guest ion in the binding site. As mentioned above, the competition between ion binding and ion solvation directly affects selectivity and efficiency of host-guest complex formation. It is difficult to disentangle effects of ion-receptor interaction and ion solvation solely through characterization of complexes in solution, since the presence of the solvent itself hinders an unobstructed view of ion-receptor binding. This problem can be circumvented by comparing vibrational spectra in different solvents with the vibrational spectrum of the same host-guest complex in vacuo. Cryogenic ion vibrational spectroscopy (CIVS) in concert with quantum chemical calculations has been very successful for the detailed spectroscopic characterization of mass-selected ions, ^{8, 28-39} including host-guest complexes of omC4P with halide ions. ³⁵ In the present work, we use infrared (IR) spectroscopy in vacuo and in solution together with density functional theory to investigate the effects of anion size and shape on ion binding to omC4P, using nitrate guest ions as a case study in comparison with chloride (see Supporting Information for a description of the methods used).

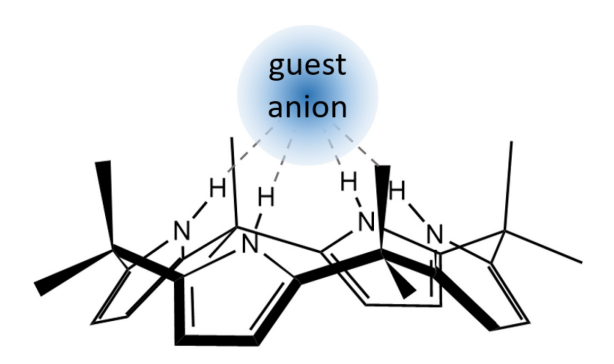


Figure 1. Structural motif of anionic guests binding to omC4P.

Comparing the calculated minimum energy structures of NO₃-omC4P and of Cl-omC4P (Figure 2), 35 one of the marked differences between omC4P complexes with halides and with NO₃ is that NO₃⁻ can, in principle, have two different binding motifs in the binding site, where the NH groups of omC4P can form H-bonds with one or two of the O atoms in NO₃⁻ (Figure 2). The isomer with a single NO group pointing into the binding site (isomer A), interacting with all four pyrrole NH groups, is calculated to be 98 meV lower in energy than the alternative geometry (isomer B), where each H-bonded NO group interacts with two NH groups. Table 1 summarizes selected properties of these structures. Interestingly, the distance from the NH groups to the bound NO group(s) in the nitrate complex is calculated to be significantly shorter than for the chloride complex, despite a higher proton affinity of Cl⁻ (ca. 1395 kJ/mol)⁴⁰ than of NO₃⁻ (ca. 1358 kJ/mol),⁴¹ and a higher calculated charge on Cl⁻ than on the bound O atom(s). We attribute this at first glance unexpected result to the size of the bound ion. For comparison, the H-O bond length in nitric acid is calculated to be 97 pm while the H-Cl bond length in hydrochloric acid is calculated to be 130 pm, consistent with the difference in H-bond lengths of the anion-receptor complexes shown in Table 1.

The ion shape and charge distribution of nitrate result in distortion of the binding sight in the nitrate complex compared to the chloride complex. The N-H-Cl angle in the chloride complex is ca. 175°, while in the nitrate complex (isomer A) the symmetry between NH groups coordinated to the bound ion is broken. The N-H-O_{bound} angles in-plane with the nitrate adduct are 159°, and the other pair are 171°. The N-H-N angles are 177° and 167° for the in-plane and out-of-plane groups, respectively, and the in-plane N-H-O_{free} angles are 153°. In other words, all four of the NH groups point nearly straight at the Cl⁻ ion, while the pyrrole rings twist in the nitrate complex toward the nearest unbound O atoms of the NO₃⁻ ion, resulting in two of the NH groups pointing

in the direction of the bound oxygen and two pointing between the bound and nearest free oxygen. The two out-of-plane pyrrole groups tilt inward toward the nitrate ion and the in-plane rings tip slightly outward. In Cl⁻·omC4P, the dihedral angle between all four pyrroles is 0°. When binding NO₃⁻, the out-of-plane and in-plane groups rotate ca. 6° out and 1° in, respectively, creating a dihedral angle of ca. 7° between adjacent pyrrole groups. In both calculated isomers, the NH-O_{bound} distances are ca. 200 pm (considering the two closest H atoms to each bound O in isomer B), which suggests approximately equal strength of the H-bonds. However, the NH-O_{free} distances in isomer A are 294 pm (nearest in-plane NH) and 357 pm (out-of-plane), while the spacing is ca. 394 pm in Isomer B. The greater proximity of the H atoms to the free O in Isomer A lends itself to stronger attractive interactions, better stabilizing the bound complex and drawing the NO₃⁻ moiety overall deeper into the binding pocket (Figure 2).

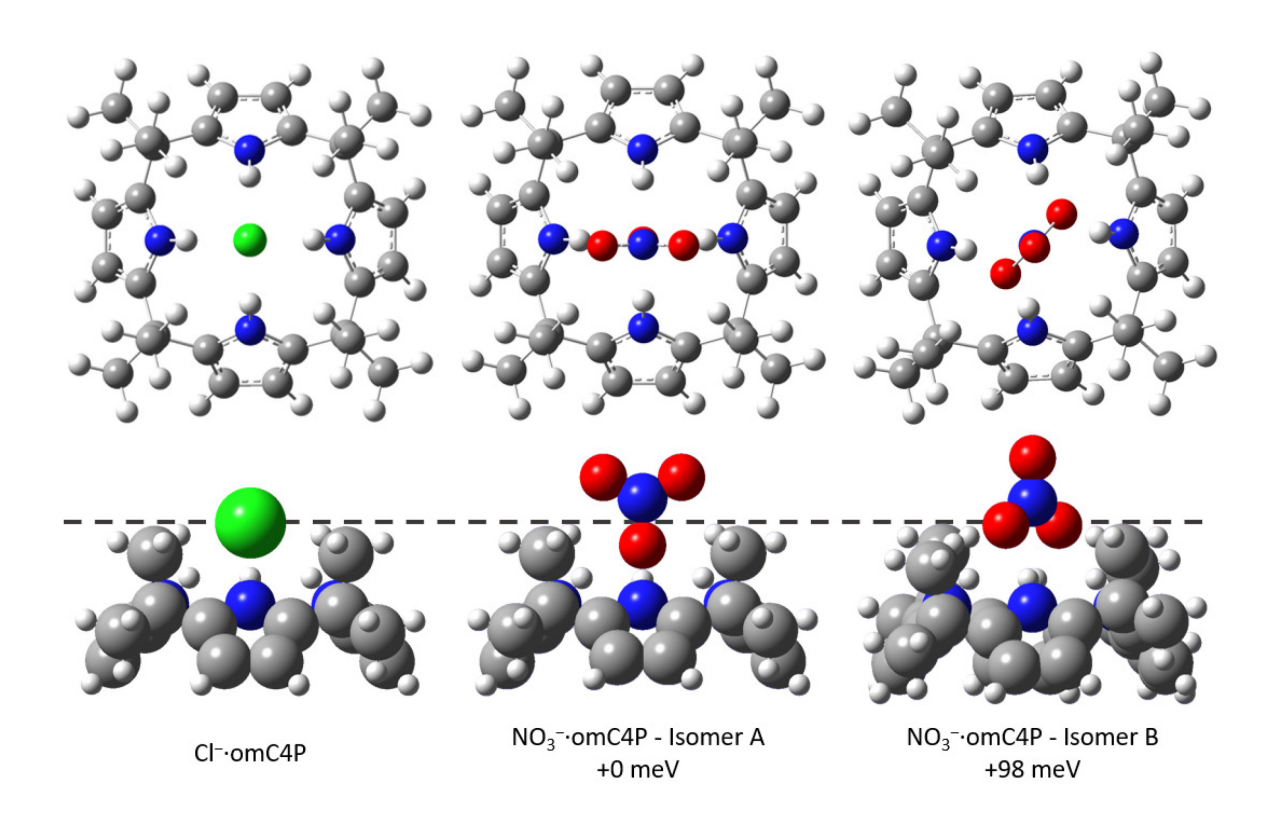


Figure 2. Calculated structures of gas-phase anion-omC4P complexes. The zero-point corrected relative energies are given for each NO_3^- ·omC4P structure. Top row: views along the symmetry axis of each complex. Bottom row: side views shown with covalent radii and a dashed line to represent the rim of the binding pocket and visualize the extent of solvent exposure. C = grey, H = white, N = blue, O = red, Cl = green.

Table 1. Selected Calculated Properties of Chloride-omC4P and Nitrate-omC4P Complexes.

guest ion	NH···ion distance [pm]	N-O distance [pm]	charge distribution in ion ^a
Cl ⁻	231 [238] ^b		-0.797 e [-0.839] ^b (total charge on Cl ⁻)
NO ₃ ⁻ isomer A	200° [205] ^b	131 (H-bonded)	-0.659 e [-0.628e] ^b (H-bonded O)
	197 ^d [203] ^b	124 (free)	-0.466 e [-0.495e] ^b (free O)
NO ₃	200	127 (H-bonded)	-0.580 e (H-bonded O)
isomer B		123 (free)	-0.444 e (free O)

^a NBO charges.

The different nature of the guest ions in Cl⁻·omC4P and NO₃⁻·omC4P is reflected in clear differences in the NH stretching region of the IR spectra of the complexes. Figure 3 shows the experimental and calculated IR photodissociation spectra of nitrogen tagged Cl⁻·omC4P³⁵ and NO₃⁻·omC4P. The shape of the nitrate ion and concomitant shifts in the macrocycle structure lower the symmetry of the complex from C_{4v} in Cl⁻·omC4P to C_{2v} in NO₃⁻·omC4P, consistent with a change in the pattern of the NH stretching modes. As shown in previous work,³⁵ the chloride complex has a feature at 3239 cm⁻¹, corresponding to two degenerate NH stretching modes with e symmetry, while the peak at 3277 cm⁻¹ is the signature of a mode with a_1 symmetry. Missing from

^b Values in square brackets are from calculations using a polarizable continuum model (PCM) with a dielectric constant of acetonitrile (35.688 as implemented in Gaussian 16).

^c NH group in NO₃ plane.

^d NH group out of NO₃ plane.

the spectrum is a symmetry-forbidden b_1 mode (see Supporting Information for the patterns of motion in each mode).

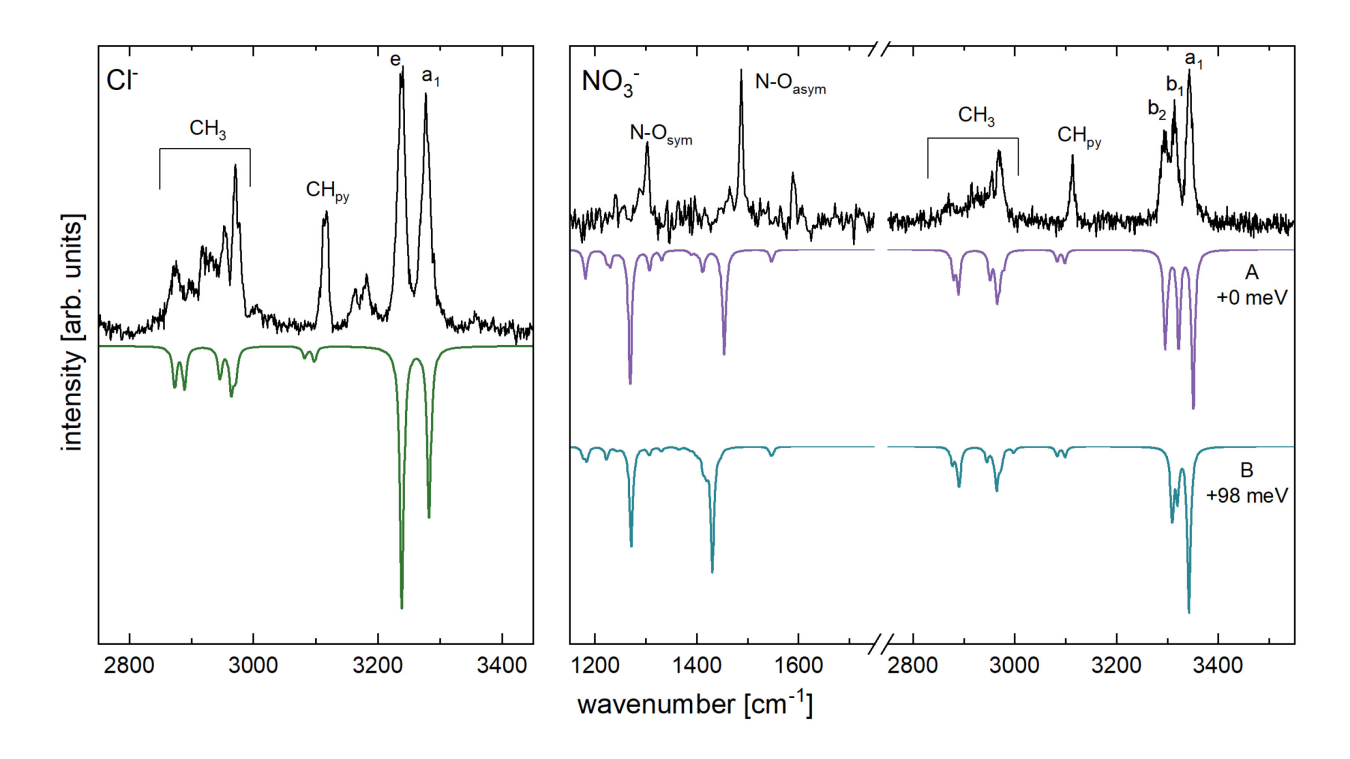


Figure 3. Experimental IR photodissociation spectra (upright) and calculated IR spectra (inverted) of Cl⁻·omC4P·N₂ (left, taken from ref. ³⁵) and of NO₃⁻·omC4P·N₂ (right). The ion is indicated in each panel and calculated traces are color coded and labeled for each conformer of the nitrate complex, including their relative energies. See text for description of peak labels.

The symmetry breaking of the anion-omC4P complex upon exchange of chloride with nitrate transforms the e modes in Cl⁻·omC4P to a b_2 mode and a b_1 mode, lifting their degeneracy. The experimental spectrum reflects this symmetry lowering, showing three prominent transitions at 3293 cm⁻¹, 3314 cm⁻¹, and 3343 cm⁻¹ (Figure 3 and Table 2). The experimental pattern fits better to the calculated spectrum for isomer A than for isomer B. Together with the fact that isomer A is

lower in energy, we therefore attribute the spectrum to isomer A, consistent with NMR and X-ray crystallography data in organic solvents.^{42, 43} Based on the narrow width of the lines in the experimental spectrum, we judge that only one isomer is present in our experiment. Attributing the experimental spectrum to isomer A, we can assign the individual transitions in the NH stretching region. The peak at 3293 cm⁻¹ corresponds to the b_2 symmetry mode characterized by the out of phase oscillation of the NH groups coplanar with the NO₃⁻ ion. The feature at 3314 cm⁻¹ is the signature of the b_1 mode, in which the other pair of NH groups oscillate out of phase. The peak at 3343 cm⁻¹ is the radially symmetric, in-phase linear combination of all four NH oscillators, resulting in a mode with a_1 symmetry. The final mode has the same pattern of motion as the symmetry-forbidden b_1 mode in Cl⁻·omC4P, but is now a weakly allowed a_1 mode (see Supporting Information). It is calculated to be at 3301 cm⁻¹, between the b_2 and b_1 NH stretching features, but at only ca. 10% of their intensities, and we do not resolve it in the experimental spectrum.

The NH(a_1) mode in the nitrate complex is blue shifted by 66 cm⁻¹ compared to the equivalent mode in the chloride complex, and the average of the antisymmetric NH(b_2) and NH(b_1) features in NO₃⁻·omC4P is blue shifted from the equivalent NH(e) transition in Cl⁻·omC4P by 65 cm⁻¹, qualitatively captured by harmonic calculations (see Table 2). This overall blue shift is due to the difference in proton affinity of the anion and also reflected in binding energy of the anion to omC4P. Chloride has a higher proton affinity of 1395 kJ/mol⁴⁰ and has a binding energy of 2.82 eV¹⁸ (calculated 2.37 eV at the present level of theory³⁵), while nitrate has a proton affinity of 1358 kJ/mol⁴¹ and calculated binding energy of 2.08 eV. Concomitantly, the weaker interaction of nitrate with the NH groups leaves the NH stretching modes closer to that of free, neutral omC4P (highest calculated, scaled harmonic value 3454 cm⁻¹, see Supporting Information).

Table 2. Selected Experimental and Scaled Harmonic Vibrational Frequencies of Chloride-omC4P³⁵ and Nitrate-omC4P Complexes in cm⁻¹.

Ion	Experimental	Harmonic	Characterization
Cl ⁻	2874, 2899 ^a	2873 - 2889 ^b	CH ₃ symmetric stretching
	$2953, 2970^{a}$	$2945 - 2972^{b}$	CH ₃ asymmetric stretching
	3113	3083	CH _{Py} antisymmetric stretching
	3118	3098	CH _{Py} symmetric stretching
	3239 (3261) ^d	3239 (3289) ^e	degenerate NH stretching (e)
	3277 (3297) ^d	3283 (3313) ^e	symmetric NH stretching (a_1)
NO ₃	1303	1269	free N–O symmetric stretching (a ₁)
	1487	1454	free N–O asymmetric stretching (b_2)
	2870, 2915 ^a	$2873 - 2889^{b}$	CH ₃ symmetric stretching
	2955, 2971 ^a	$2946 - 2971^b$	CH ₃ asymmetric stretching
	3113	3083, 3099°	CH _{Py} antisymmetric stretching
	3293 (3370) ^d	3301 (3336) ^e	antisymmetric NH stretching (b_2)
	3314 (3370) ^d	3322 (3362) ^e	antisymmetric NH stretching (b_1)
	3343 (3430) ^d	3351 (3378) ^e	symmetric NH stretching (a_1)

^a Peak centroid.

^b Range of calculated features with this character.

^c Experimental features unresolved.

^d Values in parentheses are from FTIR spectra in CD₃CN solutions, with the two features shown in Figure 4 fitted by two Gaussian profiles. The b_2 and b_1 transitions are not resolved in solution, their average position is reported here instead. See Supporting Information for FTIR data for solutions in (CD₃)₂CO.

^e Values in parentheses are from calculations in a polarizable continuum with the dielectric constant of acetonitrile (35.688 as implemented in Gaussian 16).

We assign the remaining features in the mid-IR spectrum of the nitrate complex in analogy to the case of Cl⁻·omC4P³⁵ and consistent with the scaled harmonic calculations shown in Figure 3. Exchanging Cl⁻ for NO₃⁻ has little effect on the CH stretching features, as expected from the halide-omC4P series.³⁵ The CH stretching modes of the eight methyl groups are encoded in the cluster of peaks labeled CH₃ in Figure 3 and listed in Table 2 from 2800-3000 cm⁻¹. This region is more complicated and congested than the harmonic calculations predict, most likely due to Fermi resonances with the overtones and combination bands of the methyl HCH bending modes.⁴⁴ The congestion makes detailed assignments of the peaks difficult; however, we provisionally assign the 2870 cm⁻¹ and 2915 cm⁻¹ to linear combinations of the local symmetric stretching modes of the CH₃ groups and the peaks at 2955 cm⁻¹ and 2971 cm⁻¹ to the linear combinations of asymmetric stretching modes of these groups. The peak labeled CH_{py} at 3113 cm⁻¹ is consistent with the CH stretching modes of the pyrrole groups in the spectrum of the chloride complex.³⁵

Just as the presence of the nitrate ion breaks the symmetry of the receptor, the interaction with the receptor lowers the symmetry of the nitrate ion from D_{3h} to C_{2v} . As a result, the vibrational signature of the ion in the receptor is also changed. Bare nitrate has a degenerate (e) antisymmetric stretching mode, which is observed at ca. 1356 cm⁻¹ in a Ne matrix.⁴⁵ Interaction with the receptor lifts this degeneracy. The resulting lower frequency a_1 mode is characterized by a symmetric stretching motion of the free NO groups out of phase with the stretching motion of the H-bonded NO group. The higher frequency b_2 mode corresponds to an antisymmetric stretching motion of the free NO groups with only weak stretching character in the H-bonded NO group. The experimental spectrum shows these modes at 1303 cm⁻¹ (a_1) and 1487 cm⁻¹ (b_2), respectively. The symmetric stretching mode is symmetry-forbidden in free NO₃⁻, but is calculated to be at 995 cm⁻¹ and IR allowed in the nitrate-omC4P complex, due to lowering of the local D_{3h} symmetry of the

 NO_3^- ion to $C_{2\nu}$ by the presence of the ion receptor, which is also reflected in the charge distribution in the NO_3^- ion (Table 1). This frequency is outside the range probed experimentally in the present work, and we only note the calculated frequency for completeness.

The calculated NO stretching frequencies for isomer B are very similar to those for isomer A, and the corresponding spectral region therefore cannot serve to identify the binding motif. Interestingly, the lower frequency in isomer B encodes the antisymmetric NO stretching motion of the two H-bonded NO groups, and the higher frequency component reflects a symmetric stretching motion of the two H-bonded NO groups, out of phase with the free NO group. In other words, the two vibrational modes swap their character between the two isomers (See Supporting Information).

We discuss the other observable transitions in the lower frequency range based on our identification of isomer A as the only populated structure. A feature at 1590 cm⁻¹ is due to two nearly degenerate, unresolved transitions characterized by NH bending mixed with pyrrole CC stretching motions. The weak shoulder at 1465 cm⁻¹ also has NH bending character, mixed with HCH bending motions on the CH₃ groups. A shoulder on the low frequency side (at 1287 cm⁻¹) of the symmetric NO stretching band mixes NH bending motions with pyrrole CH bending, and a weak peak at 1240 cm⁻¹ combines pyrrole CH bending and methyl wagging.

The interaction with the chemical environment of the complex, in particular with solvents, changes the binding behavior of a given ion to an ion receptor. Figure 4 shows a comparison of the spectrum of NO_3^- ·omc4P in vacuo with the spectrum in deuterated acetonitrile solution. The CH₃ stretching features are largely unaffected by the change in chemical environment, and the frequency position of the CH_{Py} signature remains unshifted as well. However, the NH stretching features shift to higher frequencies in solution. The NH(b_2) and NH(b_1) transitions are not clearly

resolved, but interpreting the peak of the broad lower frequency NH stretching feature in the solution phase spectrum as comparable to the average peak position of the two features in vacuo, the solvent-induced blue shift is 67 cm⁻¹. Similarly, the NH(a_1) peak shifts by 87 cm⁻¹. These shifts are significantly more pronounced than those found in halide-omC4P complexes, where the average blue shift of the NH(e) and NH(a_1) peaks for Cl⁻ and Br⁻ is 20-23 cm⁻¹. In order to identify the physical origins for the different shifts, we first turn to modeling solvent effects, using a polarizable continuum model (PCM).⁴⁶ While the PCM calculations qualitatively capture the solvatochromic blue shift for both Cl⁻ and NO₃⁻ guest ions, they predict very similar magnitudes of these shifts, despite a much greater solvent exposure of nitrate compared to chloride (see Figure 2). The shifts for Cl⁻ are overestimated, while they are underestimated for NO₃⁻ (see Table 2). Interestingly, the structural changes upon solvation of NO₃⁻·omC4P by acetonitrile are calculated to be smaller than for Cl⁻·omC4P (see Table 1), where the calculated change in the NH-ion distance is smaller for NO₃⁻ than for Cl⁻. An additional effect of the presence of the dielectric is a change in the charge distribution of the NO₃⁻ ion (Table 1), with the charge on the H-bonded NO group decreasing in a dielectric medium.

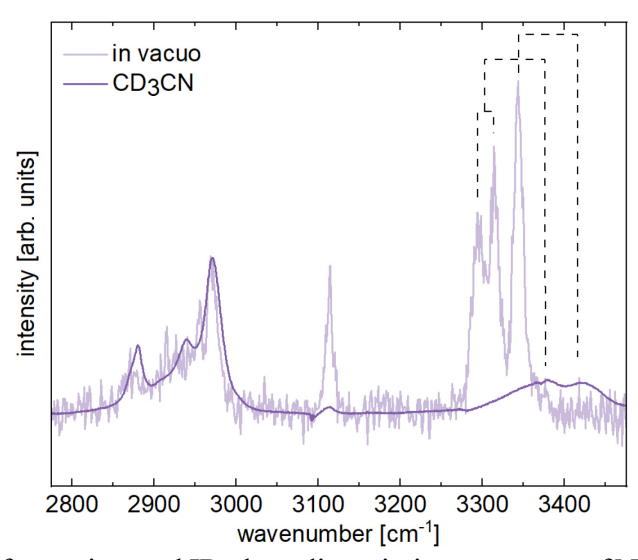


Figure 4. Comparison of experimental IR photodissociation spectrum of NO₃⁻·omC4P (faded line) with the FTIR spectrum of a 10 mM solution of NO₃⁻·omC4P in CD₃CN (thick line). The dashed lines visualize the blue shift of the NH stretching modes in solution. See Supporting Information for FTIR data of (CD₃)₂CO solution.

The discrepancies between the experiment and the PCM results, in particular the differences between chloride and nitrate complexes, highlight limitations of this computational model. We note that solvent-induced shifts appear to be smaller for deuterated acetone solutions than those in acetonitrile (see Supporting Information), qualitatively reflecting the lower dielectric constant of acetone (20.7), consistent with a significant electrostatic contribution to the observed blue shift. In principle, PCM calculations should reflect electrostatic effects, at least with a consistent trend between different guest ions. However, the PCM model does not capture molecular interactions of the ion and solvent molecules. Given the much greater solvent exposure of NO₃⁻ in the omC4P complex compared the analogous chloride complex (Figure 2), such molecular effects may be responsible for the greater experimental shift.⁴⁷

In summary, nitrate binds to omC4P through H-bonds between the four NH groups of the receptor and a single NO group of the guest ion. The geometry of the complex reflects the fact that

nitrate is not well represented by a point charge, in contrast to halide ions. Binding of a polyatomic ion results in symmetry breaking of the anion-omC4P complex. The reduced symmetry of C_{2v} for NO_3^- om C4P compared to C_{4v} symmetry in the case of the halide-om C4P complexes is clearly observed in the change in pattern of the NH stretching signatures, which encode the interaction between the anion and the omC4P binding site. These features shift to higher frequencies, consistent with the lower proton affinity of nitrate compared to chloride. Compared to halides, 35, ⁴⁷ the size of nitrate leads to a greater exposure of the guest ion to the chemical environment of the complex. This is reflected by a pronounced solvent induced shift of the NH stretching features to higher frequencies, which is on average nearly four times greater than for chloride. The magnitude of the shift increases with increasing dielectric constant, pointing to electrostatics as a significant origin of the shift. However, PCM calculations, which should capture the electrostatic contributions, are inadequate to capture the solvent effects in nitrate-omC4P beyond the most qualitative level. A quantitative description of solvent effects on the binding geometry and intermolecular forces, and by extension, of the binding selectivity for different ions in different solvents, likely requires including molecular interactions with solvent molecules more explicitly.

ASSOCIATED CONTENT

Supporting Information. The following files are available free of charge:

File 1: Methods; calculated lowest energy structure and NH stretching frequencies for neutral

omC4P; mode patters of NH stretching vibrational modes; FTIR spectra of NO₃-omC4P solutions

in d₃-acetonitrile and d₆-acetone; atomic coordinates for neutral omC4P and for NO₃⁻·omC4P.

File 2: Animations of NO vibrations in isomer A and isomer B.

AUTHOR INFORMATION

Corresponding Author

*weberjm@jila.colorado.edu

Notes

The authors declare no competing financial interests.

ACKNOWLEDGMENT

J.M.W. gratefully acknowledges support by the National Science Foundation under award no.

CHE-2154271. This work utilized resources from the University of Colorado Boulder Research

Computing Group, which is supported by the National Science Foundation (awards ACI-1532235

and ACI-1532236), the University of Colorado Boulder, and Colorado State University. We thank

Prof. Pablo Ballester and Dr. Gemma Aragay (Institut Català d'Investigació Química, Tarragona,

Spain) for helpful discussions on the chemistry of calix[4]pyrroles.

REFERENCES

- (1) Cremer, P. S.; Flood, A. H.; Gibb, B. C.; Mobley, D. L. Collaborative Routes to Clarifying the Murky Waters of Aqueous Supramolecular Chemistry. *Nature Chem.* **2018**, *10*, 8-16.
- (2) Dong, J.; Davis, A. P. Molecular Recognition Mediated by Hydrogen Bonding in Aqueous Media. *Angew. Chem. Int. Ed.* **2021**, *60*, 8035-8048.
- (3) Escobar, L.; Ballester, P. Molecular Recognition in Water Using Macrocyclic Synthetic Receptors. *Chem. Rev.* **2021**, *121*, 2445-2514.
- (4) Kubik, S. Anion Recognition in Aqueous Media by Cyclopeptides and Other Synthetic Receptors. *Acc. Chem. Res.* **2017**, *50*, 2870-2878.
- (5) Ariga, K.; Ito, H.; Hill, J. P.; Tsukube, H. Molecular Recognition: From Solution Science to Nano/Materials Technology. *Chem. Soc. Rev.* **2012**, *41*, 5800-5835.
- (6) Duax, W. L.; Griffin, J. F.; Langs, D. A.; Smith, G. D.; Grochulski, P.; Pletnev, V.; Ivanov, V. Molecular Structure and Mechanisms of Action of Cyclic and Linear Ion Transport Antibiotics. *Biopolymers* 1996, 40, 141-155.
- (7) Martínez-Crespo, L.; Sun-Wang, J. L.; Sierra, A. F.; Aragay, G.; Errasti-Murugarren, E.; Bartoccioni, P.; Palacín, M.; Ballester, P. Facilitated Diffusion of Proline across Membranes of Liposomes and Living Cells by a Calix[4]pyrrole Cavitand. *Chem* **2020**, *6*, 3054-3070.
- (8) Sato, E.; Hirata, K.; Lisy, J. M.; Ishiuchi, S.; Fujii, M. Rethinking Ion Transport by Ionophores: Experimental and Computational Investigation of Single Water Hydration in Valinomycin-K⁺ Complexes. *J. Phys. Chem. Lett.* **2021**, *12*, 1754-1758.

- (9) Sierra, A. F.; Hernández-Alonso, D.; Romero, M. A.; González-Delgado, J. A.; Pischel, U.; Ballester, P. Optical Supramolecular Sensing of Creatinine. *J. Am. Chem. Soc.* **2020**, *142*, 4276-4284.
- (10) Greer, M. A.; Goodman, G.; Pleus, R. C.; Greer, S. E. Health Effects Assessment for Environmental Perchlorate Contamination: The Dose Response for Inhibition of Thyroidal Radioiodine Uptake in Humans. *Environ. Health Perspect.* **2002**, *110*, 927-937.
- (11) Wang, Y. X.; Li, P.; Guo, Q. H.; Jiang, Z.; Liu, M. L. Environmental Biogeochemistry of High Arsenic Geothermal Fluids. *App. Geochem.* **2018**, *97*, 81-92.
- (12) Kolesnichenko, I. V.; Anslyn, E. V. Practical Applications of Supramolecular Chemistry. *Chem. Soc. Rev.* **2017**, *46*, 2385-2390.
- (13) Kubik, S.; Reyheller, C.; Stüwe, S. Recognition of Anions by Synthetic Receptors in Aqueous Solution. *J. Incl. Phenom. Macrocycl. Chem.* **2005**, *52*, 137-187.
- (14) Liu, Y.; Sengupta, A.; Raghavachari, K.; Flood, A. H. Anion Binding in Solution: Beyond the Electrostatic Regime. *Chem* **2017**, *3*, 411-427.
- (15) Sengupta, A.; Liu, Y.; Flood, A. H.; Raghavachari, K. Anion-Binding Macrocycles

 Operate Beyond the Electrostatic Regime: Interaction Distances Matter. *Chem. Eur. J.* **2018**, *24*, 14409-14417.
- (16) Allen, W. E.; Gale, P. A.; Brown, C. T.; Lynch, V. M.; Sessler, J. L. Binding of Neutral Substrates by Calix[4]pyrroles. *J. Am. Chem. Soc.* **1996**, *118*, 12471-12472.
- (17) Anzenbacher, P.; Jursíková, K.; Lynch, V. M.; Gale, P. A.; Sessler, J. L. Calix[4]pyrroles Containing Deep Cavities and Fixed Walls. Synthesis, Structural Studies, and Anion Binding

Properties of the Isomeric Products Derived from the Condensation of p-Hydroxyacetophenone and Pyrrole. *J. Am. Chem. Soc.* **1999**, *121*, 11020-11021.

- (18) Cao, W.; Wang, X. Organic Molecules Mimic Alkali Metals Enabling Spontaneous Harpoon Reactions with Halogens. *Chem. Eur. J.* 2024, e202400038.
- (19) Escobar, L.; Arroyave, F. A.; Ballester, P. Synthesis and Binding Studies of a Tetra-α Aryl-Extended Photoresponsive Calix[4]pyrrole Receptor Bearing Meso-Alkyl Substituents. *Eur. J. Org. Chem.* **2018**, *2018*, 1097-1106.
 - (20) Gale, P. A.; Sessler, J. L.; Král, V. Calixpyrroles. Chem. Commun. 1998, 1-8.
- (21) Gale, P. A.; Sessler, J. L.; Kral, V.; Lynch, V. Calix[4]pyrroles: Old Yet New Anion-Binding Agents. *J. Am. Chem. Soc.* **1996**, *118*, 5140-5141.
- (22) Gil-Ramirez, G.; Escudero-Adan, E. C.; Benet-Buchholz, J.; Ballester, P. Quantitative Evaluation of Anion-Π Interactions in Solution. *Angew. Chem. Int. Ed.* **2008**, *47*, 4114-4118.
- (23) Kim, D. S.; Sessler, J. L. Calix[4]pyrroles: Versatile Molecular Containers with Ion Transport, Recognition, and Molecular Switching Functions. *Chem. Soc. Rev.* **2015**, *44*, 532-546.
- (24) Nishiyabu, R.; Palacios, M. A.; Dehaen, W.; Anzenbacher, P. Synthesis, Structure, Anion Binding, and Sensing by Calix[4]pyrrole Isomers. *J. Am. Chem. Soc.* **2006**, *128*, 11496-11504.
- (25) Sessler, J. L.; Gale, P. A.; Genge, J. W. Calix[4]pyrroles: New Solid-Phase HPLC Supports for the Separation of Anions. *Chem. Eur. J.* **1998**, *4*, 1095-1099.
- (26) Baeyer, A. Ueber ein Condensationsproduct von Pyrrol mit Aceton. *Ber. Dtsch. Chem. Ges.* **1886**, *19*, 2184-2185.

- (27) Sessler, J. L.; Gross, D. E.; Cho, W. S.; Lynch, V. M.; Schmidtchen, F. P.; Bates, G. W.; Light, M. E.; Gale, P. A. Calix[4]pyrrole as a Chloride Anion Receptor: Solvent and Countercation Effects. *J. Am. Chem. Soc.* **2006**, *128*, 12281-12288.
- (28) Asmis, K. R.; Neumark, D. M. Vibrational Spectroscopy of Microhydrated Conjugate Base Anions. *Accounts Chem. Res.* **2012**, *45*, 43-52.
- (29) Craig, S. M.; Menges, F. S.; Duong, C. H.; Denton, J. K.; Madison, L. R.; McCoy, A. B.; Johnson, M. A. Hidden Role of Intermolecular Proton Transfer in the Anomalously Diffuse Vibrational Spectrum of a Trapped Hydronium Ion. *PNAS* **2017**, *114*, E4706-E4713.
- (30) DeBlase, A. F.; Dziekonski, E. T.; Hopkins, J. R.; Burke, N. L.; Sheng, H. M.; Kenttämaa, H. I.; McLuckey, S. A.; Zwier, T. S. Alkali Cation Chelation in Cold β-O-4 Tetralignol Complexes. *J. Phys. Chem. A* **2016**, *120*, 7152-7166.
- (31) Fischer, K. C.; Sherman, S. L.; Voss, J. M.; Zhou, J.; Garand, E. Microsolvation Structures of Protonated Glycine and L-Alanine. *J. Phys. Chem. A* **2019**, *123*, 3355-3366.
- (32) Foreman, M. M.; Terry, L. M.; Weber, J. M. Binding Pocket Response of EDTA Complexes with Alkaline Earth Dications to Stepwise Hydration-Structural Insight from Infrared Spectra. *J. Phys. Chem. A* **2023**, *127*, 5374-5381.
- (33) Nielsen, S. B.; Andersen, L. H. Properties of Microsolvated Ions: From the Microenvironment of Chromophore and Alkali Metal Ions in Proteins to Negative Ions in Water Clusters. *Biophys. Chem.* **2006**, *124*, 229-237.
- (34) Rizzo, T. R.; Boyarkin, O. V. Cryogenic Methods for the Spectroscopy of Large, Biomolecular Ions. *Top. Curr. Chem.* **2015**, *364*, 43-97.

- (35) Terry, L. M.; Foreman, M. M.; Rasmussen, A. P.; Mccoy, A. B.; Weber, J. M. Probing Ion-Receptor Interactions in Halide Complexes of Octamethyl Calix[4]Pyrrole. *J. Am. Chem. Soc.* **2024**, *146*, 12401-12409.
- (36) Tsybizova, A.; Fritsche, L.; Gorbachev, V.; Miloglyadova, L.; Chen, P. Cryogenic Ion Vibrational Predissociation (CIVP) Spectroscopy of a Gas-Phase Molecular Torsion Balance to Probe London Dispersion Forces in Large Molecules. *J. Chem. Phys.* **2019**, *151*, 234304.
- (37) Wada, K.; Kida, M.; Muramatsu, S.; Ebata, T.; Inokuchi, Y. Conformation of Alkali Metal Ion-Calix[4]Arene Complexes Investigated by IR Spectroscopy in the Gas Phase. *Phys. Chem. Phys.* **2019**, *21*, 17082-17086.
- (38) Wang, X. B.; Yang, X.; Wang, L. S. Probing Solution-Phase Species and Chemistry in the Gas Phase. *Int. Rev. Phys. Chem.* **2002**, *21*, 473-498.
- (39) Wolk, A. B.; Leavitt, C. M.; Garand, E.; Johnson, M. A. Cryogenic Ion Chemistry and Spectroscopy. *Acc. Chem. Res.* **2014**, *47*, 202-210.
- (40) Martin, J. D. D.; Hepburn, J. W. Determination of Bond Dissociation Energies by Threshold Ion-Pair Production Spectroscopy: An improved D(HCl). *J. Chem. Phys.* **1998**, *109*, 8139-8142.
- (41) Davidson, J. A.; Fehsenfeld, F. C.; Howard, C. J. Heats of Formation of NO₃⁻ and NO₃⁻ Association Complexes with HNO₃ and HBr. *Int. J. Chem. Kinet.* **1977**, *9*, 17-29.
- (42) Adriaenssens, L.; Estarellas, C.; Jentzsch, A. V.; Belmonte, M. M.; Matile, S.; Ballester,
 P. Quantification of Nitrate-π Interactions and Selective Transport of Nitrate Using
 Calix[4]pyrroles with Two Aromatic Walls. J. Am. Chem. Soc. 2013, 135, 8324-8330.

- (43) Bates, G. W.; Gale, P. A.; Light, M. E. Interactions of Organic Halide and Nitrate Salts with *meso*-Octamethylcalix[4]pyrrole. *Supramol. Chem.* **2008**, *20*, 23-28.
- (44) Schneider, H.; Vogelhuber, K. M.; Schinle, F.; Stanton, J. F.; Weber, J. M. Vibrational Spectroscopy of Nitroalkane Chains Using Electron Detachment and Ar Predissociation. *J. Phys. Chem. A* **2008**, *112*, 7498-7506.
- (45) Forney, D.; Thompson, W. E.; Jacox, M. E. The Vibrational Spectra of Molecular Ions Isolated in Solid Neon. XI. NO⁺₂, NO⁻₂, and NO⁻₃. *J. Chem. Phys.* **1993**, *99*, 7393-7403.
- (46) Miertuš, S.; Scrocco, E.; Tomasi, J. Electrostatic Interaction of a Solute with a Continuum. A Direct Utilization of Ab Initio Molecular Potentials for the Prevision of Solvent Effects. *Chem. Phys.* **1981**, *55*, 117-129.
- (47) Dean, J. L. S.; Cramer, C. G.; Fournier, J. A. Interplay between Anion-Receptor and Anion-Solvent Interactions in Halide Receptor Complexes Characterized with Ultrafast Infrared Spectroscopies. *Phys. Chem. Chem. Phys.* **2024**, *26*, 21163-21172.